# Role of microRNA-126 in vascular cognitive impairment in mice

Peng Yu[1,2,3],* ⓘ, Poornima Venkat[2],* ⓘ, Michael Chopp[2,4],
Alex Zacharek[2], Yi Shen[2], Ruizhuo Ning[2,5], Linlin Liang[2,6],
Wei Li[2], Li Zhang[2], Julie Landschoot-Ward[2], RongCai Jiang[1,7]
and Jieli Chen[2]

## Abstract

Vascular dementia (VaD) affects cognition and memory. MicroRNA-126 (miR-126) is an angiogenic microRNA that regulates vascular function. In this study, we employ a multiple microinfarction (MMI) model to induce VaD in mice, and investigate VaD-induced cognitive dysfunction, white matter (WM) damage, glymphatic dysfunction and the role of miR-126 in mediating these effects. Male six-to eight-months old C57/BL6 mice (WT) were subject to MMI model, and cerebral blood flow (CBF), vessel patency, glymphatic function, cognitive function, and serum miR-126 expression were measured. Mice were sacrificed at 28 days after MMI. To investigate the role of miR-126 in VaD, cognitive function, water channel integrity and glymphatic function were assessed in male, six-to eight months old conditional-knockout endothelial cell miR-126 (miR-126$^{EC-/-}$), and control (miR-126$^{fl/fl}$) mice. MMI in WT mice induces significant cognitive deficits, decreases CBF and vessel patency; evokes astrocytic and microglial activation, increases inflammation, axonal/WM damage; decreases synaptic plasticity and dendritic spine density, instigates water channel and glymphatic dysfunction, and decreases serum miR-126 expression. MiR-126$^{EC-/-}$ mice exhibit significant cognitive impairment, decreased CBF, myelin density and axon density, increased inflammation, and significant water channel and glymphatic dysfunction compared to miR-126$^{fl/fl}$ mice. Reduction of endothelial miR-126 expression may mediate cognitive impairment in MMI-induced VaD.

## Introduction

Vascular dementia (VaD) is a complex neurodegenerative disease affecting cognition and memory. Cognitive impairment resulting from cerebrovascular disease may result from several mechanisms, one of which involves multiple focal ischemic strokes/microinfarcts, vascular dysfunction, decrease in cerebral blood flow (CBF) and cerebral parenchymal cell damage.[1–5] Neuroimaging and neuro-pathological studies have found that microinfarction is related with cognitive decline.[6] The multiple microinfarction (MMI) model in rodents can be used to represent global decline in CBF as one contributor to VaD. The MMI model in rodents has been shown to induce axon damage, demyelination, hippocampal damage, blood–brain barrier disruption,

[1]Department of Neurosurgery, Tianjin Medical University General Hospital, China
[2]Department of Neurology, Henry Ford Hospital, Detroit, MI, USA
[3]Department of Neurosurgery, The Shanghai Tenth People's Hospital, Tongji University, Shanghai, China
[4]Department of Physics, Oakland University, Rochester, MI, USA
[5]Department of Neurology, First Hospital Harbin, Harbin, China
[6]Reproductive Medical Center, Henan Provincial People's Hospital, Zhengzhou, China
[7]Tianjin Neurological & Gerontology Institute, Key Laboratory of Post-Neurotrauma Neurorepair and Regeneration in Central Nervous System, Ministry of Education and Tianjin City, Tianjin, China

*These authors contributed equally to this work.

**Corresponding authors:**
Jieli Chen, Henry Ford Hospital Education & Research Building, 2799 W. Grand Boulevard Detroit, MI 48202, USA.
Email: jchen4@hfhs.org
Rongcai Jiang, Department of Neurosurgery, Tianjin Medical University General Hospital.
Email: jiang116216@163.com

increase inflammatory responses, impair water channel function and induce glymphatic dysfunction.[1–5]

MicroRNAs (miRs) are small non-coding RNA molecules that regulate complex biological networks at the cellular level. MiR-126 is known to exert key roles in regulating endothelial cell function, maintaining vascular integrity, accelerating post ischemic angiogenesis, as well as endovascular inflammation and platelet activation.[7,8] Endothelial injury and platelet activation result in microvascular damage either by promoting adhesion and vasoconstriction, or via thrombosis and vascular occlusion.[9] Such damage to the arteries and arterioles that supply the deep white matter (WM) of brain can result in WM infarctions.[10] Therefore, we investigate the role of miR-126 in driving pathophysiological events and cognitive deficits in MMI-induced VaD.

The glymphatic system is a functional waste clearance pathway that removes metabolic wastes and neurotoxins from the brain along paravascular channels via astroglial-mediated interstitial fluid bulk flow.[11] Aquaporin-4 (AQP-4) is predominantly present in astrocytic endfeet near capillaries and in cells lining the ventricles which are key sites for water movement between the cellular, vascular, and ventricular compartments. AQP-4 mediated water channels facilitate extensive movement of cerebrospinal fluid (CSF) into the brain parenchyma, CSF-interstitial fluid exchange, interstitial solute clearance, and post injury edema formation and resolution.[11,12] In aging, Alzheimer's disease, stroke, and diabetes, disruption of AQP-4 impairs glymphatic functioning and leads to the accumulation of metabolic waste and neurotoxins.[11,13–15] Previous studies using MMI model in rats and mice have indicated that glymphatic impairment may also play an important role in cognitive impairment and VaD pathology.[4] In this study, we investigate whether MMI in mice induces cognitive impairment and study the pathophysiological changes such as axonal/WM damage, glymphatic dysfunction, inflammatory responses, and the role of miR-126 mediating these changes.

## Material and methods

All experiments were conducted in accordance with the standards and procedures of the American Council on Animal Care and with the approval of Institutional Animal Care and Use Committee of Henry Ford Health System. Investigators were blinded to the experimental groups to perform cognitive tests and immunohistochemical analysis. The manuscript has been prepared following the ARRIVE guidelines.

### MMI model and experimental groups

Male, six-to-eight months old, C57BL/6 wild type (WT) mice were randomized to control or MMI group ($n = 8$/group). Mice were subject to MMI as previously described.[1] Briefly, mice were anesthetized with 2% isoflurane for pre-anesthetic, and spontaneously respired with 1.5% isoflurane in 2:1 $N_2O:O_2$ mixture using a facemask connected and regulated with a modified FLUOTEC 3 Vaporizer (Fraser Harlake, Orchard Park, NY) and rectal temperature maintained at 37°C. The method for preparation of cholesterol crystals has previously been described in detail.[1] To determine the optimal range of cholesterol crystals to be injected, we initially chose 3500 crystals, following previously published methods.[3,4] However, the mice when injected with 3500 crystals exhibited severe neurological deficits, and the mortality rate was >50%. We then performed dose-finding experiments with 1000, 1500, 2000, 2500, 3000 crystals and found that for 1500 crystals, the mortality rates were <20% and injection of 1500 crystals induced significant cognitive and behavioral deficits. Therefore, freshly prepared, 40–70 μm sized $1500 \pm 300$ crystals/100 μl saline/per mice were slowly injected into the right internal carotid artery via the external carotid artery, as previously described.[5] The external carotid artery was ligated after injection while the internal carotid artery remained patent. Novel object recognition (NOR) test, odor test and Morris water maze test were performed following previously described methods[1] on 21–28 days after MMI. Two sets of mice were prepared that were sacrificed at 3 days or 28 days after MMI for immunohistochemical analysis.

### Generation of miR-126[EC−/−] and miR-126^{fl/fl} mice and experimental groups

The miR-126 transgenic mouse strain (PDGFBiCreER; miR-126 flox/flox and miR-126 flox/flox) was generously provided by Dr. Calvin J. Kuo, Stanford University and has been previously described.[16–18] Four doses of tamoxifen (1 mg/10 g body weight in corn oil) were administered every other day i.p. PDGFBiCreER;miR-126 flox/flox mice develop endothelial cell miR-126 deletion which is identified as miR-126[EC−/−] at about two weeks after Tamoxifen administration. MiR-126flox/flox (MiR-126^{fl/fl}) littermate mice were employed as control. Male, six-to-eight months old, miR-126[EC−/−] and miR-126^{fl/fl} mice (age matched to WT group) were subject to a battery of cognitive tests and sacrificed for immunohistochemical analysis ($n = 8$/group). The mortality rate was zero for miR-126^{fl/fl} and miR-126[EC−/−] groups at age six-to-eight months, as these were not subject to surgery.

### CBF measurement

Regional CBF was measured in anesthetized mice using Laser Doppler flowmetry (LDF; PeriFlux PF4;

Perimed AB, Datavägen, Sweden). The apparatus displays blood perfusion signal as a color-coded image ranging from dark blue (low perfusion) to bright red (high perfusion). Using a midline scalp incision, the skull was exposed and non-contact, regional blood flow in the ipsilateral and contralateral brain hemispheres was continuously recorded for 5 min in anesthetized mice. Relative cortical blood flow values were obtained as perfusion units while maintaining consistent acquisition parameters and region of interest for all mice at all-time points of measurement.[19] Relative CBF was measured at baseline, and at 30 min and 1 day after MMI/sham surgery, and data are presented as % CBF relative to baseline values ($n = 6$/group). Data for miR-126$^{EC-/-}$ and miR-126$^{fl/fl}$ mice are presented as average CBF in perfusion units ($n = 8$/group).

## Blood pressure and blood gases measurement

Male, six-to-eight months old, C57 mice were subject to MMI or sham surgery ($n = 5$/group). Sham surgery was performed by injecting saline instead of cholesterol crystals into the right internal carotid artery via the external carotid artery. The femoral artery was cannulated using PE10 tubing with tip tapered over a flame, and blood pressure was continuously monitored using a physiological pressure transducer coupled to a data-acquisition system (ADInstruments, Australia). Arterial blood was sampled before and after sham/MMI surgery and blood gases were measured using i-STAT handheld blood gas analyzer (Abott, Chicago, IL).

## FITC perfusion

Fluorescein isothiocyanate (FITC)-dextran (FD2000S, Sigma, St. Louis, MO) at dose of 5 mg/mice in 0.2 ml PBS was injected intravenously 5 min before sacrifice at four days after MMI in an additional set of WT control and MMI mice ($n = 5$/group). Brains were immersion fixed in 4% paraformaldehyde for 48 h in 4°C and 80 µm thick coronal sections obtained using a vibratome. Whole brain sections were imaged under a 10 × objective using a laser-scanning confocal microscope (Zeiss LSM 510 NLO, Carl Zeiss, Germany).

## Glymphatic function measurement

An additional set of WT-control, WT-MMI (14 days after MMI), miR-126$^{EC-/-}$ and miR-126$^{fl/fl}$ mice were prepared ($n = 9$/group) to evaluate glymphatic function using previously described methods.[1,4,11,13,15] Mice were injected with 10 µl of 1:1 1% Texas Red-conjugated dextran (3 kD, Invitrogen, Carlsbad, CA) and 5 µl of 1% FITC-conjugated dextran (500 kD, Invitrogen, Carlsbad, CA) into the cisterna magna over 5 min using a syringe pump. Mice (three/group/time point) were sacrificed at 30 min, 1 h and 3 h after start of infusion and transcardially perfused with 0.9% saline followed by 4% paraformaldehyde; 80 µm thick vibratome coronal sections were imaged using a 10 × objective of a laser-scanning confocal microscope (Zeiss LSM 510 NLO, Carl Zeiss, Germany). MCID image analysis system (Imaging Research, St. Catharines, Ontario, Canada) was used to quantify the fluorescence density and data are presented as % of positive fluorescence area in the brain cross section.

## Immunohistochemistry

Following transcardial perfusion with 0.9% saline, brains were immersion fixed in 4% paraformaldehyde. A standard paraffin block was obtained, and every 10th coronal section for a total of 5 sections (6 µm thick) was used for immunohistochemical staining. To study early inflammatory changes in the brain after MMI, antibodies against Glial fibrillary acidic protein (GFAP, 1:10,000; Dako, Santa Clara, CA), and Ionized calcium binding adaptor molecule 1 (IBA1, microglia and monocyte marker, 1:1000, Wako, Mountain View, CA) were used in mice sacrificed at three days after MMI. To study late WM/axonal damage, Bielschowsky silver (BS) and Luxol fast blue (LFB) staining was used for quantification of axons and myelin, respectively, and antibodies against FITC-labeled AQP-4 (1:1500, EMD Millipore, Burlington, MA), adenomatous polyposis coli (APC, Oligodendrocyte marker, 1:100, GenWay, San Diego, CA), neuron-glial antigen 2 (NG2, Oligodendrocyte progenitor cell marker, 1:400, EMD Millipore, Burlington, MA) and synaptophysin (synaptic protein, 1:400, Abcam, Cambridge, United Kingdom) were used in mice sacrificed at 28 days after MMI. Myelin basic protein (MBP, 1:400; Dako, Santa Clara, CA) and phosphorylated neurofilament heavy chain (pNFH, 1:1500; Covance, Princeton, NJ) double staining were used for representative images of myelin and axon, respectively. DAPI immunofluorescence staining was used to stain nuclei. Prussian blue staining and hematoxylin and eosin (H&E) staining were used to evaluate hemorrhage.[20,21] For control experiments, non-immune serum was substituted for the primary antibody.

## Quantification analysis

Although cholesterol crystals were injected unilaterally into the right ICA, WM/axonal damage was observed

in both the hemispheres, which is consistent with our previous study[1] as well as other studies.[3,4] Therefore, for each brain, five slides with each containing eight fields of view of ipsi- and contralateral striatum and corpus callosum were digitized under a $20 \times$ or $40 \times$ objective (Olympus BX40, Tokyo Japan) using a three-CCD color video camera (Sony DXC-970MD) interfaced with MCID image analysis system (Imaging Research, St. Catharines, Ontario, Canada). For each field of view, positive cell numbers were counted, or the positive stained area was measured using built-in densitometry function with a density threshold above unstained set uniformly for all groups. Data were averaged to obtain a single value for each animal and presented as percentage positive area or number of positive cells/mm$^2$.

### Golgi silver staining

An additional set of WT-control and WT-MMI mice (4/group) were sacrificed three days after MMI for Golgi staining (Rapid Golgi stain kit, FD Neuro-Technologies, Columbia, MD). Primary branching of 10 intact neurons per slide was counted in the layer III of cortex under a $40 \times$ objective. Neurite spine density was measured under an oil immersion $100 \times$ objective and 10 intact neurons per slide were chosen in layer III of cortex and CA3 region of hippocampus.

### Laser capture micro-dissection

Brain tissue sections ($n = 6$) from WT mice were mounted on polyethylene naphthalate (PEN) membrane slides (Leica Microsystems, Wetzlar, Germany), and stained with vWF (1:50, Dako, Santa Clara, CA) to identify endothelial cells. Brain tissue sections from miR-126$^{EC-/-}$ and miR-126$^{fl/fl}$ mice ($n = 6$/group) were also stained with vWF (1:50, Dako, Santa Clara, CA) to identify endothelial cells, and with GFAP (1:500, Dako, Santa Clara, CA) to identify astrocytes and NeuN (1:50, Millipore, Billerica, MA) to identify neurons. DAPI counterstain was employed to stain nuclei. For WT mice, endothelial cells and random brain sections consisting of endogenous brain cell types were cut from the membranes into a tube containing QIAzol (Qiagen, Hilden, Germany) using a Leica LMD6000 Microsystem (Leica Microsystems, Wetzlar, Germany).[22] For miR-126$^{fl/fl}$ and miR-126$^{EC-/-}$ groups, endothelial cells, astrocytes, and neurons were isolated using LCM similar to above procedure. Approximately 3000 positive cells for each cell type per section were isolated ($n = 6$/group). Eppendorf tubes containing QIAzol and membrane sections were later isolated for PCR following standard protocol for the miRNAeasy kit (Qiagen).

### MicroRNA measurement

MiR expression level in the blood serum was measured as previously described.[23] Briefly, total RNA was isolated using TRIzol (Invitrogen, Carlsbad, CA) and miRNeasy Mini kit (Qiagen, Hilden, Germany). RT-PCR was then used to detect specific miR expression levels. MiRNAs were reverse transcribed with the iRNA Reverse Transcription kit (Applied Biosystems, Foster City, CA) and PCR amplification was performed with the hsa-miR-126-3 p TaqMan miRNA assay kit (Applied Biosystems, Foster City, CA), which is specific for mature miRNA sequences, according to the manufacturer's protocols, with U6 snRNA as an internal control.

### Real-time PCR

Total RNA was isolated with TRIzol (Invitrogen, Carlsbad, CA) to make cDNA using the M-MLV (Invitrogen, Carlsbad, CA) standard protocol and to run a quantitative PCR using the SYBR Green real-time PCR method on a ViiA-7 PCR instrument (Applied Biosystems, Foster City, CA) using three-stage program parameters provided. Each sample was tested in triplicate, and analysis of relative gene expression data using the $2^{-\Delta\Delta CT}$ method. The following primers (Invitrogen, Carlsbad, CA) were used:

Matrix metalloproteinase-9 (MMP9): FWD: ATC TCT TCT AGA GAC TGG GAA GGA G; REV: AAG CTG ATT GAC TAA AGT AGC TGG A.

Toll like receptor-4 (TLR4): FWD: TCT AAC TTC CCT CCT GAG ATG G; REV: ACT GGC TAG AGA GCA AGA GGA A.

### Statistical analysis

One-way analysis of variance (ANOVA) was used for the evaluation of cognitive function tests and histology, respectively. "Contrast/estimate" statement was used to test the group difference. If an overall treatment group effect was detected at $p < 0.05$, pair-wise comparisons were made. All data are presented as mean $\pm$ standard deviation (SD).

## Results

### MMI decreases CBF and reduces vessel patency in WT mice

Laser Doppler flowmetry was employed to assess whether MMI decreases CBF. The laser Doppler images in Figure 1(a) and FITC-Dextran perfused cerebral vasculature visualized in Figure 1(b) show that MMI decreases cortical CBF and decreases perfusion
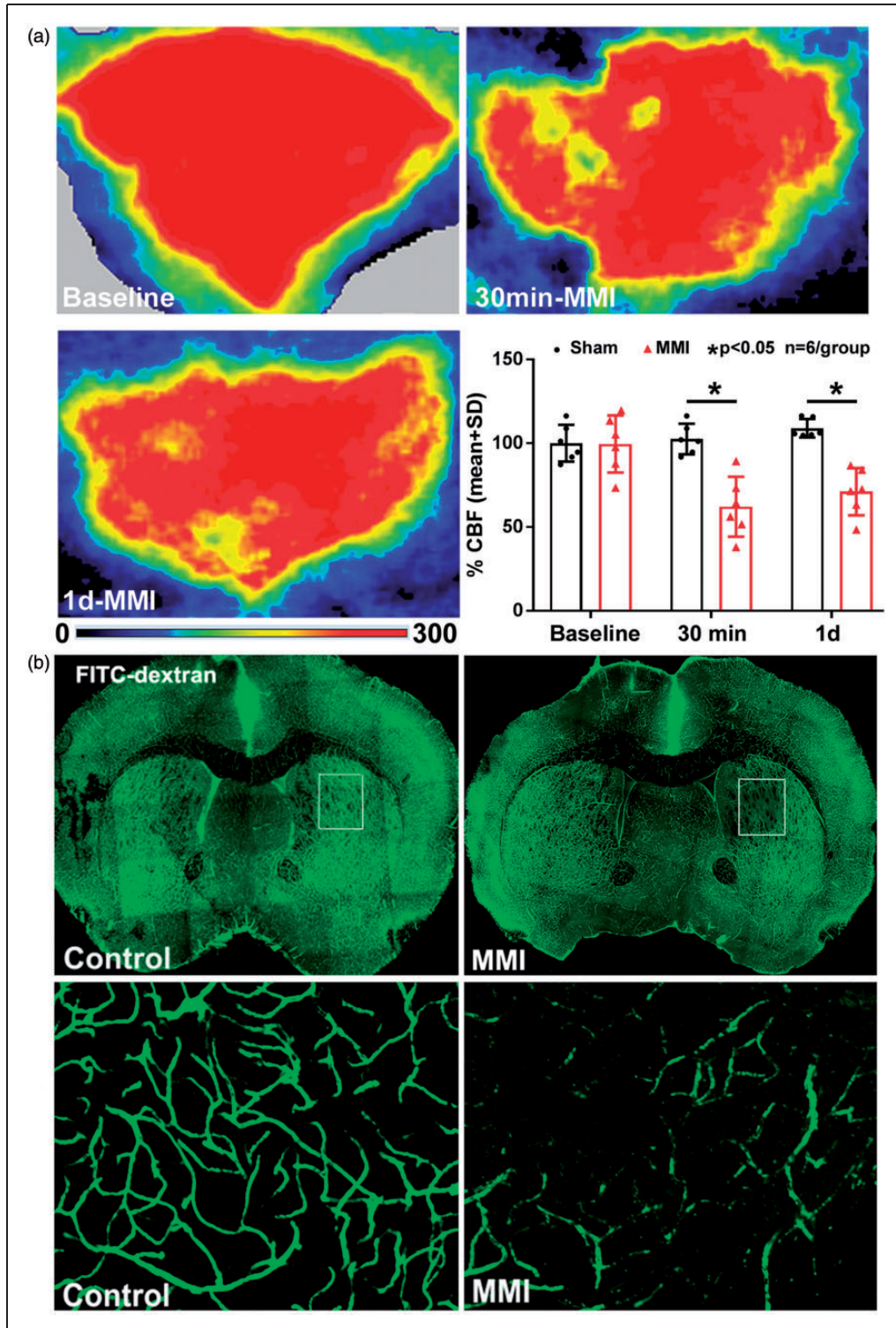
**Figure 1.** In wild type mice, (a) MMI decreases CBF at 30 min and one day after MMI and (b) decreases vessel patency in the corpus callosum and striatum in the brain at four days after MMI.

and vessel patency in the corpus callosum and in the striatum compared to WT control mice. Our data in Table 1 show that there were no significant changes in blood pressure or blood gases before and after

sham or MMI or between sham and MMI groups. To exclude the possibility of hemorrhagic events due to cholesterol crystals injection, we evaluated hemorrhage using Prussian blue as well as H&E

**Table 1.** Hemodynamic measurements.

| Group | Body weight (g) | Arterial BP (mmHg) | Heart rate (BPM) | pH | pCO$_2$ | pO$_2$ | BEecl | HCO$_3$ | TCO$_2$ | SO$_2$% |
|---|---|---|---|---|---|---|---|---|---|---|
| Pre-Sham | 29.25 ± 2.1 | 87.07 ± 6.35 | 351 ± 71 | 7.25 ± 0.16 | 31.1 ± 16.41 | 97 ± 42.01 | −14.75 ± 1.9 | 12.65 ± 1.16 | 13.5 ± 1.95 | 95 ± 3.29 |
| Post-Sham | 29.25 ± 2.1 | 94.39 ± 26.77 | 360 ± 69 | 7.18 ± 0.16 | 29.67 ± 9.16 | 108.67 ± 68.18 | −12.67 ± 3.24 | 13.833 ± 2.86 | 14.33 ± 3.24 | 95 ± 5.93 |
| Pre-MMI | 30.8 ± 2.68 | 89.01 ± 14.78 | 361 ± 67 | 7.34 ± 0.07 | 22.12 ± 7.49 | 136.2 ± 21.17 | −14 ± 2.55 | 11.72 ± 2.93 | 12.2 ± 3.04 | 99 ± 0.02 |
| Post-MMI | 30.8 ± 2.68 | 73.86 ± 14.09 | 371 ± 69 | 7.22 ± 0.12 | 24.76 ± 11.29 | 108.2 ± 19.69 | −17.2 ± 6.61 | 10.46 ± 5.41 | 11.2 ± 5.57 | 96.8 ± 1.29 |

Note: Blood pressure and blood gas measurements collected immediately before and after sham or MMI surgery in WT mice indicate that there were no significant hemodynamic changes before and after sham or MMI or between sham and MMI groups. Data are presented as mean + SD, n = 5/group.

immunostaining.[20] We did not find any incidence of hemorrhage in control or WT-MMI groups.

## MMI induces significant cognitive deficits in WT mice

To test the effects of MMI model on cognition and memory in mice, a battery of cognitive tests were performed 21–28 days after MMI. MMI in WT mice significantly decreases discrimination index in NOR and odor test indicating poor short term and long-term memory compared to control mice (Figure 2(a)). MMI in WT mice significantly impairs spatial learning and memory as indicated by significantly increased escape latency to hidden platform as well as lesser time spent in the target platform quadrant in the Morris water maze test (Figure 2(a)).

## MMI significantly increases astrocyte and microglial activity and inflammation in WT mice

Immunohistochemistry was used to test whether MMI in WT mice triggers astrocyte and microglial activation in the brain at three days after MMI. Figure 2(b) and (c) shows MMI significantly increases the expression of GFAP (marker for astrocyte activation) and IBA1 (marker for microglia) compared to WT mice. To test whether MMI regulates inflammatory factor expression in the brain, MMP9 and TLR4 expression were measured by real-time PCR. Figure 2(d) shows that MMI in mice significantly increases MMP9 and TLR4 expression in the brain compared to WT mice.

## MMI significantly increases axonal/WM damage in WT mice

To evaluate the effects of MMI on WM integrity, axon density, myelin density, and oligodendrocyte and oligodendrocyte progenitor cell numbers were quantified in WT-control and WT-MMI mice sacrificed at 28 days after MMI. Immunostaining and quantification analysis shows that MMI significantly decreases axon (BS and pNFH staining) and myelin (LFB and MBP staining) density in the WM tracts of corpus callosum and WM bundles in the striatum (Figure 3(a) and (b)), and decreases oligodendrocyte (APC) and oligodendrocyte progenitor cell (NG2) number in the striatum (Figure 3(c) and (d)) compared to normal WT control mice.

## MMI significantly decreases synaptic plasticity in WT mice

To evaluate whether MMI in WT mice impairs early and late synaptic plasticity, Golgi staining at 3 days after MMI and synaptic protein expression
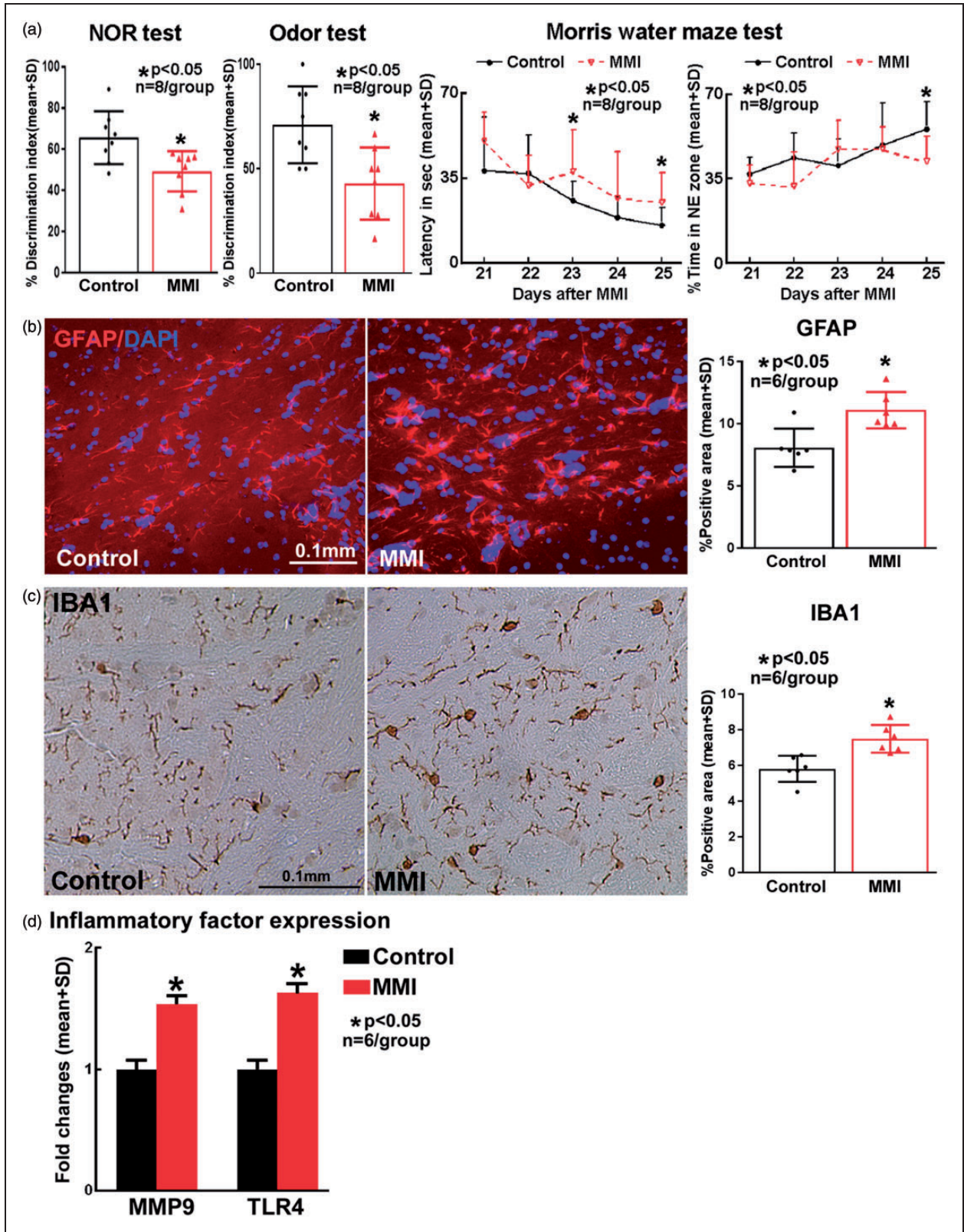
**Figure 2.** Compared to wild type control, mice subject to MMI model exhibit significant (a) learning and memory deficits at 28 days after MMI; and (b) astrocyte activation; (c) microglial activation and (d) increased brain inflammatory factor gene expression at three days after MMI.
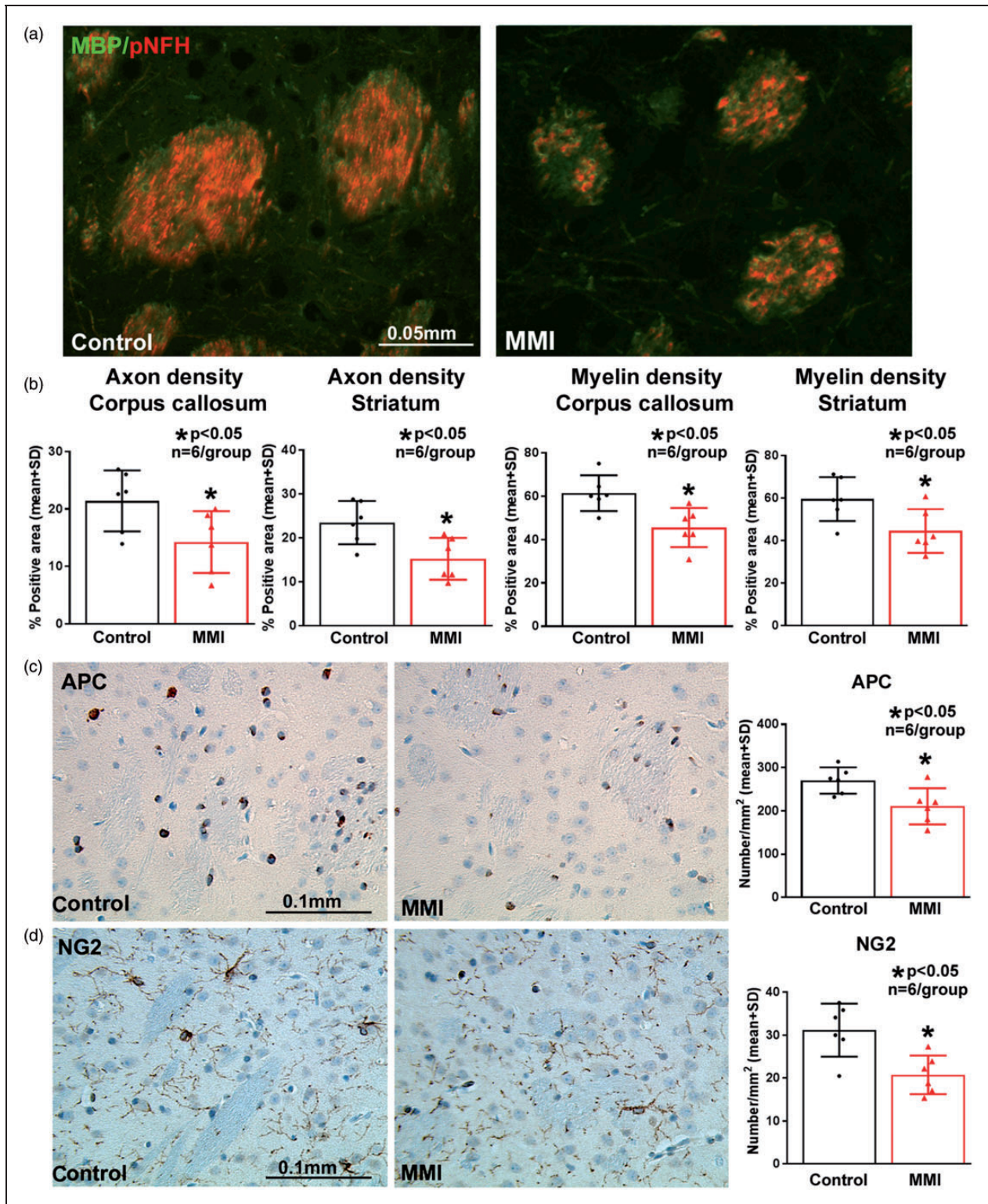
**Figure 3.** MMI in mice significantly decreases (a–b) axon and myelin density in corpus callosum and striatal white matter, (c) number of oligodendrocytes (APC) and (d) oligodendrocyte progenitor cells (NG2) in the striatum at 28 days after MMI compared to control mice.

(Synaptophysin) at 28 days after MMI were employed. Compared to WT control mice, WT-MMI mice exhibit significantly decreased Synaptophysin expression (Figure 4(a)), and decreased neuronal dendritic branching and spine density as indicated by Golgi silver staining and quantification analysis (Figure 4(b)).

## MMI induces significant water channel and glymphatic impairment in WT mice

To investigate the mechanism of MMI-induced WM damage and cognitive dysfunction, AQP4 expression and glymphatic system function were evaluated. In WT mice subject to MMI, AQP-4 expression around blood vessels was significantly decreased compared to WT control (Figure 4(c)). Ex-vivo time sequence fluorescence imaging of coronal brain sections was used to quantify movement of tracers injected into the CSF to evaluate glymphatic function. Compared to WT control mice, CSF penetration and clearance from the brain were significantly delayed in WT-MMI mice indicating glymphatic dysfunction, as shown in Figure 4(d).

## MMI significantly decreases serum miR-126 expression

To investigate whether MMI in WT mice regulates miR expression, several miR's (miR-29 a, miR-29 b, miR-29 c, miR-126, miR-181 c) associated with cognitive impairment and dementia were measured.[24,25] Among these, MMI in WT mice significantly decreases serum expression of miR-126 compared to WT control group (Figure 5(a)).

## MiR-126 is predominantly expressed in endothelial cells in mouse brain and is significantly reduced in miR-126$^{EC-/-}$ mice compared to miR-126$^{fl/fl}$ mice

LCM allows the isolation of a homogeneous cell population of a particular cell type from multiple cell types within tissue for gene expression analysis. Therefore, we isolated endothelial cells and random sections of brain tissue consisting of a mixture of endogenous brain cell types from WT mice and measured miR-126 expression. Supplementary Figure 1(a) to (d) shows that in WT mice, miR-126 expression is significantly higher in brain endothelial cells compared to brain tissue consisting of a mixture of endogenous brain cell types. We also isolated endothelial cells, astrocytes and neurons from brain tissue sections of miR-126$^{EC-/-}$ and miR-126$^{fl/fl}$ mice and measured miR-126 expression. Supplementary Figure 1(e) shows that miR-126 expression is significantly decreased in endothelial cells isolated from miR-126$^{EC-/-}$ mice brain compared to miR-126$^{fl/fl}$ mice brain sections indicating that miR-126 knockdown is primarily in endothelial cells in the brain of miR-126$^{EC-/-}$ mice.

## MiR-126$^{EC-/-}$ mice exhibit significant CBF reduction, cognitive impairment, inflammatory responses and WM damage compared to miR-126$^{fl/fl}$ mice

A battery of cognitive tests was performed on miR-126$^{EC-/-}$ and miR-126$^{fl/fl}$ mice. Figure 5(b) shows that miR-126$^{EC-/-}$ mice have significant short term, long term and spatial learning and memory deficits compared to control miR-126$^{fl/fl}$ mice. In addition, miR-126$^{EC-/-}$ mice also have significant reduction in CBF as indicated in Figure 5(a).

To investigate the effects of miR-126 decrease on inflammatory responses, astrocyte, and microglia expression was measured using immunostaining analysis and MMP9 and TLR4 expression was measured using PCR. Figure 5(a), (c) and (d) shows that miR-126$^{EC-/-}$ mice have significantly increased expression of GFAP, IBA1, MMP9 and TLR4 in the brain compared to control miR-126$^{fl/fl}$ mice.

To test whether miR-126 decrease is related to WM damage, axon and myelin density were measured in the corpus callosum and WM bundles in striatum. Figure 6(a) and (b) shows that miR-126$^{EC-/-}$ mice exhibit significantly reduced axon and myelin density compared to miR-126$^{fl/fl}$ mice.

## MiR-126$^{EC-/-}$ mice exhibit significant water channel and glymphatic impairment compared to miR-126$^{fl/fl}$ mice

To test whether miR-126 decrease affects glymphatic function, water channel and glymphatic function were tested in miR-126$^{EC-/-}$ and miR-126$^{fl/fl}$ mice. Figure 6(c) and (d) shows that miR-126$^{EC-/-}$ mice have significantly lower AQP-4 expression around blood vessels as well as exhibit glymphatic dysfunction with delayed penetration and clearance of CSF into the brain parenchyma via paravascular pathways.

## Discussion

VaD results from a decrease in blood flow to deep WM in the brain and microinfarcts are commonly found in the elderly and in patients suffering from cognitive deficits.[6] Prior studies have shown that MMI-induced microinfarcts are distributed in the cortical or sub-cortical regions, especially in the striatum, thalamus and hippocampus.[2,4,26] However, corresponding data on CBF alterations are lacking. In this study, we have shown that MMI in mice decreases CBF and induces hypoperfusion in the brain, decreases vessel patency, impairs cognition and memory, triggers inflammatory
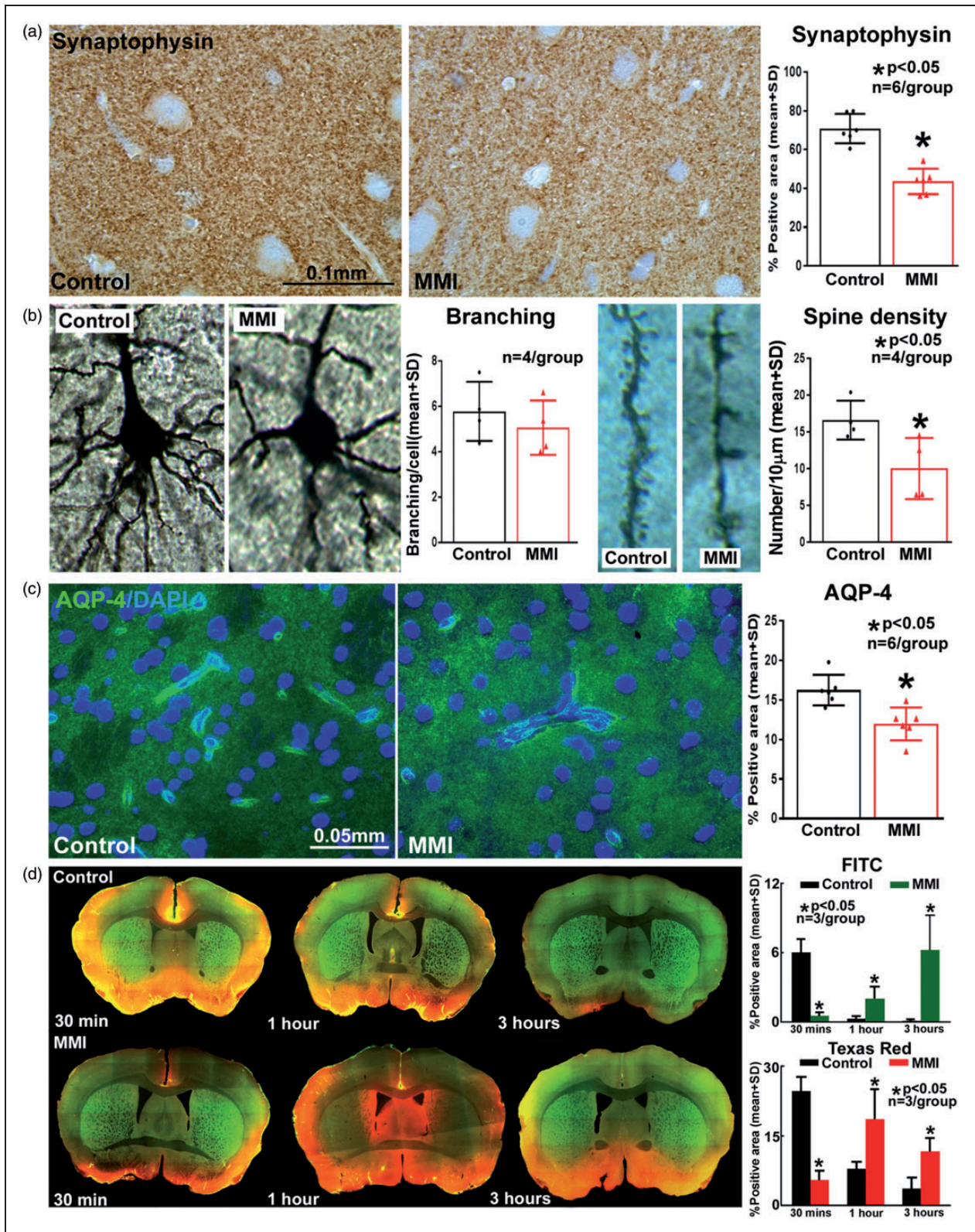
**Figure 4.** MMI in mice significantly decreases (a) synaptic protein expression at 28 days after MMI, (b) neuronal dendritic branching and spine density at 3 days after MMI, (c) Aquaporin-4 expression around cerebral blood vessels and (d) impairs cerebrospinal fluid penetration and clearance from the brain compared to wild type control mice at 14 days after MMI.
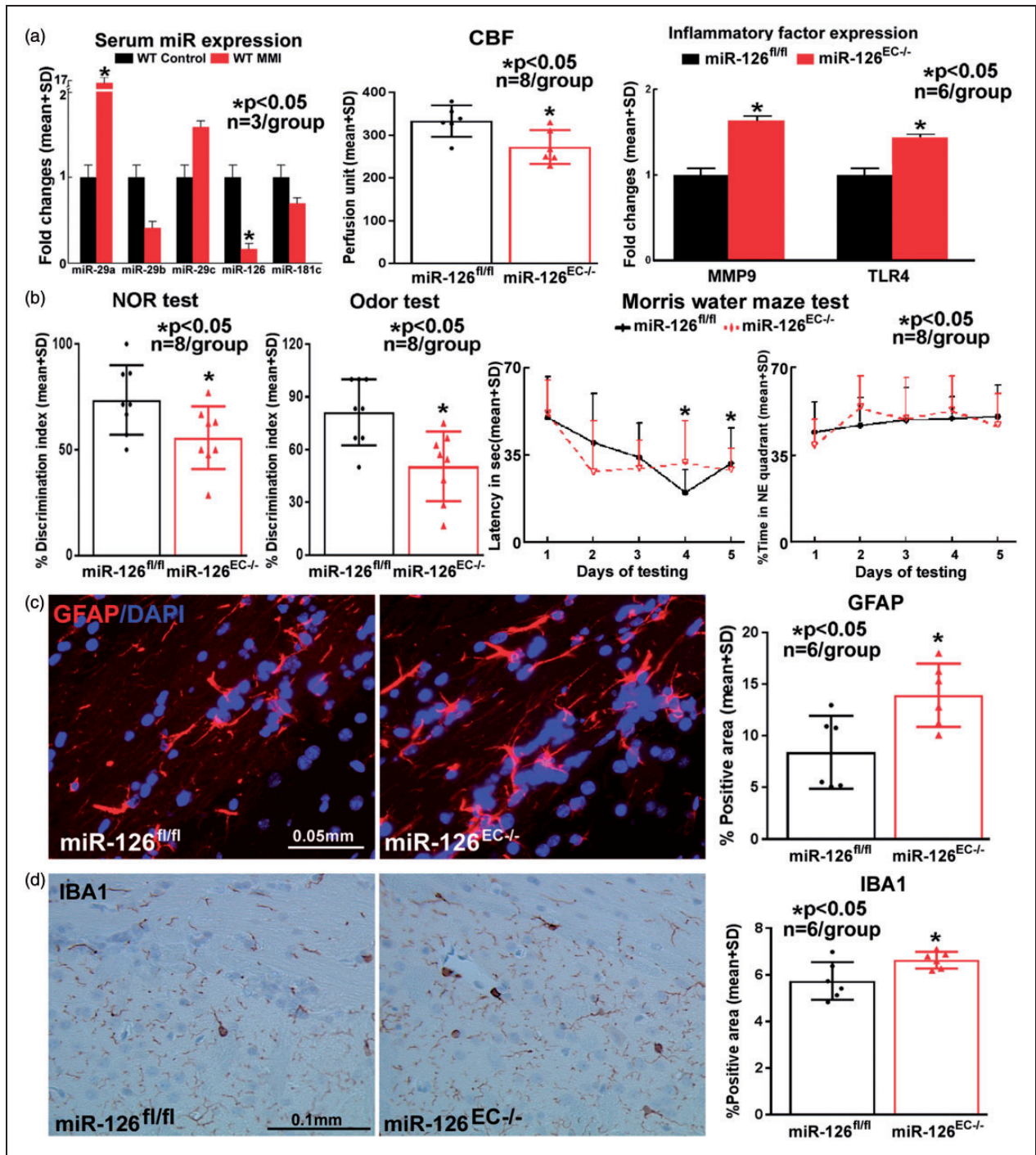
**Figure 5.** (a) MMI in mice significantly decreases serum miR-126 expression. Compared to miR-126^{fl/fl} mice, miR-126[EC−/−] mice exhibit significant CBF reduction, and increase in brain inflammatory factor MMP9 and TLR4 gene expression. Compared to miR-126^{fl/fl} mice, miR-126[EC−/−] mice exhibit significant (b) learning and memory impairment, and (c–d) increased astroglial and microglia activation.

responses, damages WM, and impairs water channel and glymphatic function compared to WT mice. These findings are in accordance with our previous results as well as other studies.[1,3,4] In this study, we report for the first time that MMI significantly decreases serum miR-126 expression compared to WT control mice, and miR-126[EC−/−] mice exhibit cognitive impairment, inflammatory responses, WM damage as well as water channel and glymphatic dysfunction compared to miR-126^{fl/fl} mice. Our data suggest that MMI
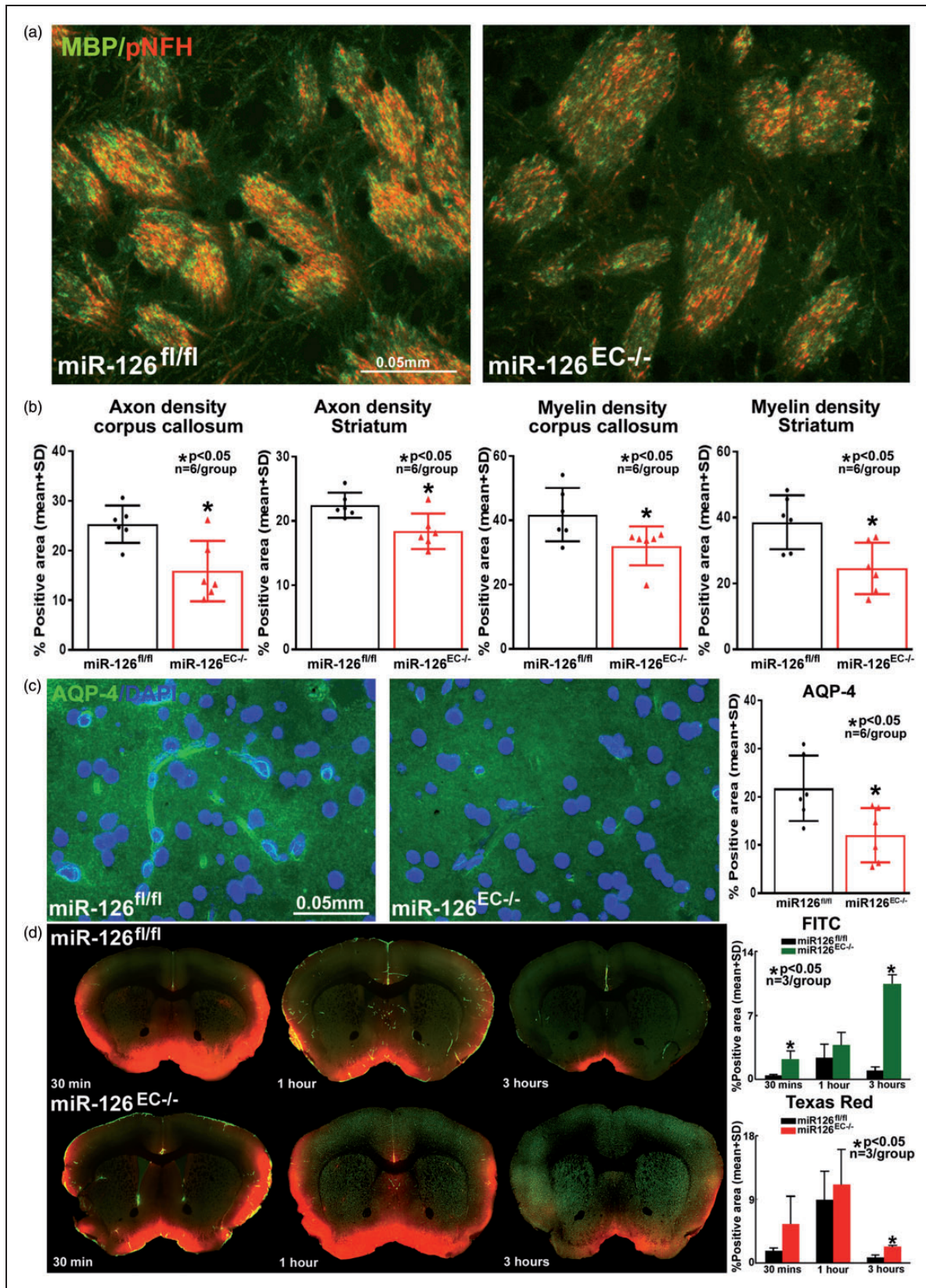
**Figure 6.** Compared to miR-126$^{fl/fl}$ mice, miR-126$^{EC-/-}$ mice have (a–b) significantly decreased axon and myelin density in the corpus callosum and striatal white matter; (c) significantly lower expression of AQP-4 around cerebral blood vessels; and (d) significant glymphatic dysfunction as indicated by significantly decreased cerebrospinal fluid penetration and delayed clearance from the brain.

in mice induces VaD which may be mediated at least in part by decreasing miR-126 expression.

There is a close relationship between miR-126 expression and WM integrity/function.[23,27] Up-regulation of miR-126 with intrathecal injections of agomir-126 significantly improved vascularity at injury site, decreased inflammatory responses and protected WM integrity in rats with spinal cord injury.[27] Inhibition of miR-126 expression in human umbilical cord blood cells (HUCBCs) significantly attenuated HUCBC-induced vascular and WM remodeling, anti-inflammatory effects and neurological function in diabetic stroke mice.[23] We found significant alteration in miR-126 expression, and to test the effects of decreasing miR-126, we compared cognitive ability and WM integrity of miR-126$^{EC-/-}$ mice and miR-126$^{fl/fl}$ mice. Our results show that MMI significantly decreases serum miR-126 expression, and miR-126 knockdown mice exhibit significant cognitive impairment, myelin rarefaction and axonal loss in corpus callosum and striatum. Overall, these data suggest that decreasing miR-126 may lead to WM damage and increased inflammatory responses in the brain.

VaD in humans is associated with lacunar infarction, loss of WM integrity, vacuolization and demyelination in the periventricular region.[28] Such damage to the periventricular WM can disrupt neuronal networks connecting to the frontal lobe which can lead to cognitive impairment.[29] Failure of remyelination and WM disease progression occurs due to impaired survival, proliferation, migration, recruitment, and differentiation of oligodendrocyte progenitor cells.[30] Synaptogenesis, synaptic plasticity and dendritic spines play an important role in memory.[31] Our data indicate that MMI induces significant myelin rarefaction, demyelination, axon degradation, decrease in oligodendrocytes and oligodendrocyte progenitor cells, decreased synaptophysin expression, neuronal branching and dendritic spine density which may contribute to cognitive impairment.

Neuroinflammatory factors secreted by reactive glial cells damage oligodendrocytes and worsen demyelination.[32,33] Accordingly, prior studies have demonstrated that MMI induces microglial and astroglial activation adjacent to sites of microinfarction in the striatum and corpus callosum at three days after MMI.[3,4] In Alzheimer's disease and mild cognitive impairment, microglial and astrocytic activation and clustering around sites of Aβ deposition create an inflammatory environment that is hostile to brain cells and induces neuronal cell death.[32,33] Cumulatively, these studies suggest an inhibitory effect of microglial and astroglial activation upon cognition. Decreasing miR-126 has been associated with inflammatory responses and increasing miR-126 has been reported to significantly attenuate microglial activation in spinal cord injury.[27] The results of our current study

show that microglial activation as well as MMP9 and TLR4 inflammatory factor expression were significantly increased in WT-MMI as well as in miR-126 knockout mice. Therefore, it is likely that MMI-induced decrease in miR-126 expression may play an important role in MMI-induced neuroinflammation.

The glymphatic system removes metabolic waste and neurotoxins from the brain along paravascular channels via astroglial-mediated interstitial fluid bulk flow.[11] Glymphatic dysfunction is reported in aging, diabetes, Alzheimer's disease, VaD, and stroke and is implicated in neurodegeneration and cognitive decline.[1,4,11,13–15] AQP-4 lined water channels facilitate waste clearance by providing a low-resistance pathway for fluid movement across the brain parenchyma.[11] AQP-4 knockout mice exhibit delayed CSF influx and ~70% reduction in interstitial solute clearance, indicating that decrease in AQP-4 in the injured brain aggravates glymphatic dysfunction.[11,12] In the present study, our results show that MMI in WT mice significantly decreases AQP-4 expression around blood vessels and impairs glymphatic functioning with delayed CSF influx as well as delayed clearance along paravascular channels. These results are consistent with previous reports indicating water channel dysfunction with decreased AQP-4 expression around blood vessels and glymphatic dysfunction with delayed global CSF influx in a traumatic brain injury as well as in VaD induced using MMI model.[1,4,12] The decrease in CBF and reduced vessel patency could contribute to the delayed entrance and clearance of CSF. Recently, Wang et al.[4] demonstrated that MMI-induced global glymphatic dysfunction was transient, and in two-to-three months old young mice subject to MMI, glymphatic dysfunction observed at 3 days after MMI resolved by 14 days after MMI.[4] While our results show that MMI-induced glymphatic dysfunction is significant at 14 days after MMI, it is likely that the delayed persistence is due to the difference in age of mice employed in our study (six-to-eight months). Wang et al.[4] have also reported that MMI-induced glymphatic dysfunction worsens with advancing age. Our results are the first to indicate water channel and glymphatic system dysfunction in miR-126 knockout mice compared to miR-126$^{fl/fl}$ mice. It is still unclear how miR-126 affects glymphatic functioning. Direct evidence indicating that AQP-4 is one of the targets of miR-126 is lacking; however, it has been demonstrated that both MMP9, a main target of miR-126,[34] and AQP-4, are involved in brain edema after injury to the brain.[35] Moreover, MMP9-induced β-Dystroglycan cleavage could disturb AQP-4 polarization which can then affect glymphatic functioning.[36] Therefore, it is likely that miR-126 indirectly regulates AQP-4 expression and affects glymphatic function in WT mice subject to MMI.

There are several limitations and unanswered questions. We have employed late adult (six-to-eight months old) male mice with no prior vascular pathologies. This does not accurately reflect true clinical situation, and future studies with aged (>18 months) male and female mice are warranted. The coupling and time sequence of pathological events such as inflammation, miR-126 decrease, WM damage, water channel and glymphatic dysfunction contributing to VaD are not yet well characterized. Further studies to obtain quantitative CBF measurements and corresponding WM changes following MMI induction over a time course of several weeks using MRI are warranted. While there is ongoing debate on the physiological function of the glymphatic system and its mechanisms,[37,38] it is well accepted that paravascular spaces around cerebral vessels offer a low-resistance pathway for convective clearance of solutes from the brain.[37] Our data indicate that alterations to this paravascular space and AQP-4 expression potentially affect water channel function and impair solute clearance from the brain after MMI in WT mice, and loss of miR-126 may mediate these effects. In our current study, we have not investigated the physiological role of the glymphatic system. In this study, among the various tested miR's, we found that MMI significantly altered miR-126 expression and therefore we tested the effect of miR-126 in cognition, WM damage and glymphatic functioning. It is likely that other miR-s also regulate various pathophysiological aspects of VaD. MiR-126 not only regulates angiogenesis and WM remodeling, but can also regulate innate immune response and inflammation.[27,39] We cannot exclude a possible contribution of the immune/inflammatory system to VaD. In this study, we have focused on the most direct physiological contributors to VaD. We acknowledge that it is likely that miR-126 modulates expression of multiple genes and signaling pathways, and future studies are warranted to delineate underlying molecular mechanisms of MMI-induced VaD.

## Conclusions

MMI in mice significantly decreases CBF, decreases miR-126 expression, induces WM damage, triggers neuroinflammatory responses, impairs glymphatic functioning and results in cognitive deficits. Knockdown of miR-126 significantly induces cognitive deficits, WM damage, neuroinflammation, and glymphatic dysfunction. Therefore, decreasing miR-126 may partially contribute to MMI-induced cognitive deficits.

## Declaration of conflicting interests

The author(s) declared no potential conflicts of interest with respect to the research, authorship, and/or publication of this article.

## Authors' contributions

PY performed experiments, analyzed data and wrote the manuscript, PV performed experiments, analyzed data, prepared figures and wrote the manuscript, MC was involved in experimental design and gave final approval of manuscript, AZ performed experiments, YS performed experiments, RN performed experiments, LL performed experiments, WL performed experiments, LZ performed experiments, JLW performed experiments, RJ was involved in experimental design and gave final approval of manuscript, JC was involved in experimental design, wrote the manuscript, analyzed data and gave final approval of manuscript

## Supplementary material

Supplementary material for this paper can be found at the journal website: http://journals.sagepub.com/home/jcb

## ORCID iD

Peng Yu https://orcid.org/0000-0002-4781-746X
Poornima Venkat https://orcid.org/0000-0001-8938-663X

## References

1. Venkat P, Chopp M, Zacharek A, et al. White matter damage and glymphatic dysfunction in a model of vascular dementia in rats with no prior vascular pathologies. *Neurobiol Aging* 2017; 50: 96–106.
2. Rapp JH, Pan XM, Neumann M, et al. Microemboli composed of cholesterol crystals disrupt the blood-brain barrier and reduce cognition. *Stroke* 2008; 39: 2354–2361.
3. Wang M, Iliff JJ, Liao Y, et al. Cognitive deficits and delayed neuronal loss in a mouse model of multiple microinfarcts. *J Neurosci* 2012; 32: 17948–17960.
4. Wang M, Ding F, Deng S, et al. Focal solute trapping and global glymphatic pathway impairment in a murine model of multiple microinfarcts. *J Neurosci* 2017; 37: 2870–2877.
5. Venkat P, Chopp M and Chen J. Models and mechanisms of vascular dementia. *Exp Neurol* 2015; 272: 97–108.
6. Kovari E, Gold G, Herrmann FR, et al. Cortical microinfarcts and demyelination affect cognition in cases at high risk for dementia. *Neurology* 2007; 68: 927–931.
7. Fish JE, Santoro MM, Morton SU, et al. miR-126 regulates angiogenic signaling and vascular integrity. *Dev Cell* 2008; 15: 272–284.

8. Wei XJ, Han M, Yang FY, et al. Biological significance of miR-126 expression in atrial fibrillation and heart failure. *Braz J Med Biol Res* 2015; 48: 983–989.

9. Shih AY, Blinder P, Tsai PS, et al. The smallest stroke: occlusion of one penetrating vessel leads to infarction and a cognitive deficit. *Nat Neurosci* 2013; 16: 55–63.

10. Brun A. Pathology and pathophysiology of cerebrovascular dementia: pure subgroups of obstructive and hypoperfusive etiology. *Dementia* 1994; 5: 145–147.

11. Iliff JJ, Wang M, Liao Y, et al. A paravascular pathway facilitates CSF flow through the brain parenchyma and the clearance of interstitial solutes, including amyloid beta. *Sci Transl Med* 2012; 4: 147ra111.

12. Iliff JJ, Chen MJ, Plog BA, et al. Impairment of glymphatic pathway function promotes tau pathology after traumatic brain injury. *J Neurosci* 2014; 34: 16180–16193.

13. Kress BT, Iliff JJ, Xia M, et al. Impairment of paravascular clearance pathways in the aging brain. *Ann Neurol* 2014; 76: 845–861.

14. Gaberel T, Gakuba C, Goulay R, et al. Impaired glymphatic perfusion after strokes revealed by contrast-enhanced MRI: a new target for fibrinolysis? *Stroke* 2014; 45: 3092–3096.

15. Jiang Q, Zhang L, Ding G, et al. Impairment of the glymphatic system after diabetes. *J Cereb Blood Flow Metab* 2017; 37: 1326–1337.

16. Claxton S, Kostourou V, Jadeja S, et al. Efficient, inducible Cre-recombinase activation in vascular endothelium. *Genesis* 2008; 46: 74–80.

17. Chen J, Cui C, Yang X, et al. MiR-126 Affects brain-heart interaction after cerebral ischemic stroke. *Transl Stroke Res* 2017; 8: 374–385.

18. Kuhnert F, Mancuso MR, Hampton J, et al. Attribution of vascular phenotypes of the murine Egfl7 locus to the microRNA miR-126. *Development* 2008; 135: 3989–3993.

19. Liu XS, Fan B, Szalad A, et al. MicroRNA-146a mimics reduce the peripheral neuropathy in type 2 diabetic mice. *Diabetes* 2017; 66: 3111–3121.

20. Liu S, Grigoryan MM, Vasilevko V, et al. Comparative analysis of H&E and Prussian blue staining in a mouse model of cerebral microbleeds. *J Histochem Cytochem* 2014; 62: 767–773.

21. Yan T, Venkat P, Chopp M, et al. Neurorestorative therapy of stroke in type two diabetes rats treated with human umbilical cord blood cells. *Stroke* 2015; 46: 2599–2606.

22. Kassis H, Shehadah A, Li C, et al. Class IIa histone deacetylases affect neuronal remodeling and functional outcome after stroke. *Neurochem Int* 2016; 96: 24–31.

23. Chen J, Ning R, Zacharek A, et al. MiR-126 contributes to human umbilical cord blood cell-induced neurorestorative effects after stroke in type-2 diabetic mice. *Stem cells* 2016; 34: 102–113.

24. Hébert SS, Horré K, Nicolaï L, et al. Loss of microRNA cluster miR-29a/b-1 in sporadic Alzheimer's disease correlates with increased BACE1/β-secretase expression. *Proc Natl Acad Sci U S A* 2008; 105: 6415–6420.

25. Fang C, Li Q, Min G, et al. MicroRNA-181c Ameliorates cognitive impairment induced by chronic cerebral hypoperfusion in rats. *Mol Neurobiol* 2017; 54: 8370–8385.

26. Rapp JH, Hollenbeck K and Pan XM. An experimental model of lacunar infarction: embolization of microthrombi. *J Vasc Surg* 2008; 48: 196–200.

27. Hu J, Zeng L, Huang J, et al. miR-126 promotes angiogenesis and attenuates inflammation after contusion spinal cord injury in rats. *Brain Res* 2015; 1608: 191–202.

28. Erkinjuntti T, Benavente O, Eliasziw M, et al. Diffuse vacuolization (spongiosis) and arteriolosclerosis in the frontal white matter occurs in vascular dementia. *Arch Neurol* 1996; 53: 325–332.

29. Sultzer DL, Mahler ME, Cummings JL, et al. Cortical abnormalities associated with subcortical lesions in vascular dementia. Clinical and position emission tomographic findings. *Arch Neurol* 1995; 52: 773–780.

30. Maki T, Liang AC, Miyamoto N, et al. Mechanisms of oligodendrocyte regeneration from ventricular-subventricular zone-derived progenitor cells in white matter diseases. *Front Cell Neurosci* 2013; 7: 275.

31. Okano H, Hirano T and Balaban E. Learning and memory. *Proc Natl Acad Sci U S A* 2000; 97: 12403–12404.

32. Solito E and Sastre M. Microglia function in Alzheimer's disease. *Front Pharmacol* 2012; 3: 14.

33. Acosta C, Anderson HD and Anderson CM. Astrocyte dysfunction in Alzheimer disease. *J Neurosci Res* 2017; 95: 2430–2447.

34. Mathiyalagan P, Liang Y, Kim D, et al. Angiogenic mechanisms of human CD34+ stem cell exosomes in the repair of ischemic hindlimb. *Circ Res* 2017; 120: 1466–1476.

35. Cao S, Zhu P, Yu X, et al. Hydrogen sulfide attenuates brain edema in early brain injury after subarachnoid hemorrhage in rats: possible involvement of MMP-9 induced blood-brain barrier disruption and AQP4 expression. *Neurosci Lett* 2016; 621: 88–97.

36. Yan W, Zhao X, Chen H, et al. beta-Dystroglycan cleavage by matrix metalloproteinase-2/-9 disturbs aquaporin-4 polarization and influences brain edema in acute cerebral ischemia. *Neuroscience* 2016; 326: 141–157.

37. Smith AJ, Yao X, Dix JA, et al. Test of the 'glymphatic' hypothesis demonstrates diffusive and aquaporin-4-independent solute transport in rodent brain parenchyma. *eLife* 2017; 6: pii: e27679.

38. Jin B-J, Smith AJ and Verkman AS. Spatial model of convective solute transport in brain extracellular space does not support a "glymphatic" mechanism. *J Gen Physiol* 2016; 148: 489–501.

39. Ferretti C and La Cava A. miR-126, a new modulator of innate immunity. *Cell Mol Immunol* 2014; 11: 215–217.